Exploring the growth mechanism of CuSbSe$_2$ thin film prepared by electrodeposition[*]

WANG Ruihu[1], BI Jinlian[1]**, LI Wei[1]**, YUAN Yujie[1], XING Yupeng[1], and YAO Liyong[2]

1. *Tianjin Key Laboratory of Film Electronic and Communication Devices, School of Integrated Circuit Science and Engineering, Tianjin University of Technology, Tianjin 300384, China*

2. *Tianjin Institute of Power Source, Tianjin 300384, China*

Copper antimony selenium (CuSbSe$_2$) has advantages of adjustable band gaps from 1.09 eV to 1.2 eV, high light absorption coefficient ($>10^5$ cm^{-1}), and low grain generation temperature (300—400 °C), which is suitable for the preparation of solar cells. However, the stable range of CuSbSe$_2$ (CASe) phase is narrow, which is inevitable to form Sb$_2$Se$_3$ and Cu$_3$SbSe$_4$ second phase during the preparation process. In this work, selenization annealing of Sb/Cu metal layer to prepare CASe thin films with pulse electrodeposition process was studied, and the growth mechanism of CASe film was analyzed. Cu and Sb reacted with Se to form Cu$_2$Se and Sb$_2$Se$_3$, respectively. Then Cu$_2$Se and Sb$_2$Se$_3$ further reacted to generate CASe. Since the formation temperature of Cu$_3$SbSe$_4$ was lower than that of CASe, the preferential formation of Cu$_3$SbSe$_4$ led to layer separation. When the annealing temperature was too high, CASe decomposed to form Cu$_3$SbSe$_3$ and Sb$_2$Se$_3$. Additionally, by increasing the heating rate, the separation of CASe thin films was effectively improved, and the CASe thin films with relatively high crystallinity were obtained at 360 °C with heating rate of 30 °C/min and selenization time of 20 min.

Cu(In,Ga)Se$_2$ (CIGS) thin film solar cells have high photoelectric conversion efficiency with the champion laboratory efficiency of 23.35%[1,2]. However, In and Ga elements are relatively scarce in the earth, which increases the cost and limits its commercial development[3]. CuSbSe$_2$ (CASe) has the advantages of earth abundant composition elements, low cost, non-toxic, and environmentally friendly. The structure of CASe crystal is two-dimensional with orthorhombic system, covalent bond connected within the layer and van der Waals force between layers, which is similar to graphene and MoS$_2$[4,5]. It is reported that Shockley-Quaythur limit efficiency of CASe is exceeded by 30%[6]. Theoretical calculation showed that the 5s^2 lone pair effect on Sb^{3+} made it a high light absorption coefficient, which was about 10^5 cm^{-1}[6]. Besides, the melting point of CASe is only 480 °C, which is much lower than that of CdTe, CIGS, and Cu$_2$ZnSnS$_4$ (CZTS) (1 093 °C, 986 °C, and 820 °C, respectively). Micron sized grains can be obtained at 300—400 °C[7,8], whose property can reduce the energy consumption during annealing.

At present, many studies of CASe absorber layer have been done to improve the efficiency of CASe thin film solar cells[9-21]. WELCH et al[13] prepared a series of CASe films at 380 °C to 410 °C by sputtering Sb$_2$Se$_3$/Cu$_2$Se. The film grown at 380 °C has the best device efficiency of (3.12±0.41)%. By controlling the flux ratio of Sb$_2$Se$_3$/Cu$_2$Se sputtered to control the synthesis gradient, a thin film solar cell with an energy conversion efficiency of 4.7% was obtained. This is the highest efficiency CASe thin film solar cell known at present[14], which is far below the Shockley-Quaythur limited efficiency and the champion efficiency of CIGS. The increased defect concentration caused by stoichiometric shift is one of the important reasons for the failure to prepare high-performance CASe thin film solar cells. It was predicted by theoretical calculation that the Cu-Sb-Se ternary system had relatively complex compositions with seven stable ternary phases[22], namely Cu$_3$SbSe$_3$, Cu$_{12}$Sb$_4$Se$_{13}$, Cu$_3$SbSe$_4$, CASe, Cu$_4$SbSe$_5$, Cu$_5$Sb$_4$Se$_6$ and Cu$_6$SbSe$_7$. However, the latter three Cu$_4$SbSe$_5$, Cu$_5$Sb$_4$Se$_6$ and Cu$_6$SbSe$_7$ are not found in nature. The phases of Cu$_3$SbSe$_3$, Cu$_{12}$Sb$_4$Se$_{13}$, Cu$_3$SbSe$_4$, CASe have been listed in the inorganic crystal structure database. Due to the narrow stable range of CASe phase, Sb$_2$Se$_3$ and Cu$_3$SbSe$_4$ and other second phase formed in CASe during the annealing process, causing the defect concentration increase. Besides, the temperature of producing Cu$_3$SbSe$_4$ was lower than that of CASe, the preferential formation of Cu$_3$SbSe$_4$ leads to layer separation, which was not conducive to carrier transport.

**   E-mails: bijinlian815@126.com; Cliwei618@126.com

There are many methods to prepare CASe, such as magnetron sputtering[13,23], continuous evaporation[16,24], hydrazine solution[15], pulsed laser deposition[18,20,25], and electrodeposition[11,21]. In the above methods, the electrodeposition has the advantages of fast deposition rate and high material utilization rate[26], which can be used to prepare CASe thin films. TANG et al[11] prepared CASe thin films on SnO_2-coated glass substrate by one-step electrodeposition and rapid thermal annealing. The suitable deposition potential is determined to be about −0.40 V. Absorption coefficient, band gap and carrier concentration of the annealed film were tested. ABOUABASSI et al[21] studied the influence of the annealing temperature on the structural, morphological, compositional and optical properties of CASe thin films electrodeposited in a single step. The formation of pure CASe phase occurs in the range 250—350 °C. From 400 °C to 500 °C, due to the partial decomposition of CASe and the antimony losses, the formation of copper-rich phases such as Cu_3SbSe_3 and Cu_3SbSe_4 increased. However, the mechanism of phase formation of CASe thin film and the layer separation mechanism based on electrodeposition followed by selenization process were not yet systematically explored.

In this work, CASe thin films were prepared by pulse electrodeposition followed by selenization. The growth mechanism and layer separation of CASe thin films were studied and analyzed in detail. A series of CASe thin films were prepared with different annealing temperatures (280—420 °C), selenization time (2—50 min) and heating rates (10—30 °C/min). The dependence of phase composition, structure and morphology of the films on annealing temperature and selenization time were studied. Finally, the CASe thin films with relatively simple composition and good crystallization degree were obtained.

Mo layer was deposited on soda lime glass by direct-current (DC) sputtering as back contact electrode. Then the Mo substrates were put into alcohol to ultrasonic clean for 30 min, and then ultrasonic clean in deionized water for 20 min. The electrolytes of Cu layer and Sb layer used in this paper were $CuSO_4$ solution and $SbCl_3$ solution, respectively. Wash the Mo substrate with a large amount of deionized water, then immediately put it into the $SbCl_3$ solution to deposit Sb layer. The deposited Sb layer was washed with deionized water and then put into $CuSO_4$ solution to deposit Cu layer. The pulse frequency of Sb and Cu was set at 10 000 Hz, the pulse duty ratio was 25%, and the pulse current density was 62.5 mA/cm². $SbCl_3$ solution was composed of 0.3 M $SbCl_3$ and 2.2 M HCl. $CuSO_4$ solution was composed of 0.8 M $CuSO_4 \cdot 5H_2O$ and 0.76 M H_2SO_4. The electric quantities of Cu and Sb are 8C and 18C, respectively. Pulse current was provided by GKPT-FB4-24 V/10 A pulse/DC power supply produced by Shicheng Company in Shenzhen, China. The process diagram of electrodepositing metal Cu and the square wave pulse current waveform used in this work are shown in Fig.1.
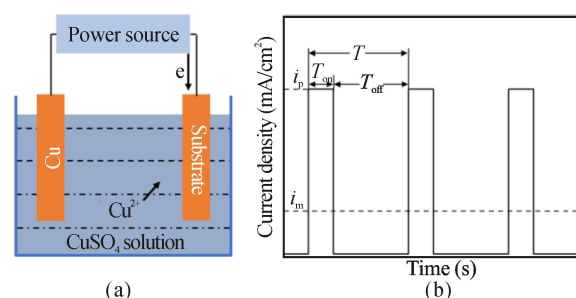
Fig.1 Schematic diagrams of (a) Cu electrodeposition process and (b) square wave pulse current waveform

Mo/Sb/Cu substrates and selenium powder were placed in different temperature zones of double-temperature zone tube furnace to prepare CASe thin films. Ar gas was filled into tube furnace for 10 min to empty the air in the pipe. The metal precursors were annealed by two-step selenization process. The temperature of Mo/Sb/Cu substrate was raised to 250 °C with heating rate of 10 °C/min and kept at 300 °C for 10 min, then raised to 360 °C and kept at 360 °C for 30 min. The selenium was heated to 300 °C with heating rate of 10 °C/min and kept at 300 °C for 50 min. After naturally cooling to room temperature, CASe film was taken out of the tube furnace.

The phase structure of the thin films was analyzed by UItima IV X-ray diffractometer (XRD) made by Rigaku Corporation Company in Japan and Renishaw inVia Reflex Raman spectrometer of Renishaw Company in UK. XRD uses Cu target as anode target, and the test angle range is 3°—120°. The excitation wavelength of the Raman spectrometer is 532 nm. The surface, cross section and element distribution of CASe thin films were tested by QuantaFEG250 field emission scanning electron microscope (FE-SEM) and energy dispersive spectroscopy (EDS) of FEI company.

Fig.2 shows the XRD patterns of CASe thin films prepared with different annealing temperatures. It can be observed that the film annealed at 280 °C contains monomeric Sb and Cu_2Se. The diffraction peaks at 28.85°, 42.13° and 51.86° correspond to the metal Sb (JCPDS: 85-1323), which did not react due to the insufficient temperature. The diffraction peaks at 27.21°, 45.09° and 53.32° correspond to the Cu_2Se phase (JCPDS: 88-2043), the reaction equation for the formation of Cu_2Se is as follows[16]

$$2Cu(s)+Se(g) \rightarrow Cu_2Se(s). \tag{1}$$

The phases of the film annealed at 300 °C includes Cu_3SbSe_4 (JCPDS: 85-0003), Sb_2Se_3 (JCPDS: 89-0821), Cu_2Se, and monomeric Sb. Although the annealing temperature was only increased by 20 °C, the intensity of Cu_3SbSe_4 peaks at 27.35°, 45.43°, 53.87°, and 54.04° was strong. A few Sb_2Se_3 peaks were also observed at 31.52° and 32.47°. The band gap of Cu-rich Cu_3SbSe_4 was about 0.4 eV[27] with a high carrier concentration of about 10^{19} cm^{-3}, which would severely deteriorate the device performance[28]. The decrease of Sb and Cu_2Se

peak intensities proved that more Sb and Cu_2Se were involved in the reaction, leading to form Sb_2Se_3 and Cu_3SbSe_4. At 300 °C, Cu_3SbSe_4 and Sb_2Se_3 began to form according to the following reactions[15]

$$4Sb(s)+3Se_2(g) \rightarrow 2Sb_2Se_3(s), \qquad (2)$$

$$3Cu_2Se(s)+Sb_2Se_3(s)+2Se(g) \rightarrow 2Cu_3SbSe_4(s). \qquad (3)$$
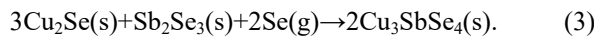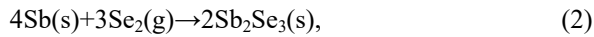
By increasing the annealing temperature to 320 °C, it was found that CASe (200) and (013) (JCPDS: 75-0992) was formed with diffraction peaks at 27.95° and 28.63°. The preferred orientation of CASe was changed, and the CASe (200) peak was stronger than the CASe (013) peak. The main peak intensity of Cu_3SbSe_4 at 27.35° gradually increased, and the peaks of monomeric Sb and Cu_2Se disappear, indicating that Sb and Cu_2Se reacted at this temperature. It was also observed that the main peak of Sb_2Se_3 at 31.52° was enhanced, and some less intense Sb_2Se_3 peaks appeared at 16.95°, 33.95°, 34.21° and 46.14°. The reaction to form CASe above 320 °C is listed as follows[16]

$$Cu_2Se(s)+Sb_2Se_3(s) \rightarrow 2CuSbSe_2(s). \qquad (4)$$

Further increasing the annealing temperature to 340 °C and 360 °C, Cu_3SbSe_4 still dominates and the CASe peaks at 27.95° and 28.63° are enhanced, indicating the improved crystallinity of CASe. A shift of the preferred orientation of CASe prepared at 380 °C is evident with the appearance of CASe (002) at 11.63° and CASe (304) at 48.94°. Moreover, part of CASe decomposed with the increase of annealing temperature, Sb_2Se_3 generated, resulting in the enhancement of Sb_2Se_3 peak intensity. The main peak intensity of Cu_3SbSe_4 at 27.35° was decreased.

The decomposition of CASe was intensified with the increase of annealing temperature, and the selective orientation changed to CASe (002) and (304), CASe (200) and (013) diffraction peaks disappeared. The reaction of CASe decomposition is shown below[18]

$$3CuSbSe_2(s) \rightarrow Cu_3SbSe_3(s)+Sb_2Se_3(g)\uparrow. \qquad (5)$$
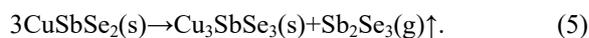
The saturated vapor pressure of Sb_2Se_3 products was large with the film annealed at and above 400 °C[29], which was volatilized sufficiently from the film, inducing to form holes in the film. The holes further exacerbated the above decomposition reaction. The Sb_2Se_3 was not detected in the subsequent XRD. The diffraction peak of Cu_3SbSe_3 (JCPDS: 86-1751) at 23.88° became very sharp, which further demonstrated the decomposition reaction of CASe. Cu_3SbSe_3, with carrier concentration of up to 10^{19} cm^{-1} like Cu_3SbSe_4, would seriously deteriorate the performance of CASe thin film solar cells.

Raman scattering spectroscopy was employed to further analyze the physical structure of the films, as shown in Fig.3. It can be seen that the characteristic vibrational peaks of Sb were observed at 117 cm^{-1} and 148 cm^{-1}, and Cu_2Se was at 260 cm^{-1} for the film annealed at 280 °C[30,31]. With the increase of annealing temperature,

the intensity of the vibrational peaks of Sb and Cu_2Se decreases. Sb and Cu_2Se completely disappeared when the annealing temperature increased to 320 °C.
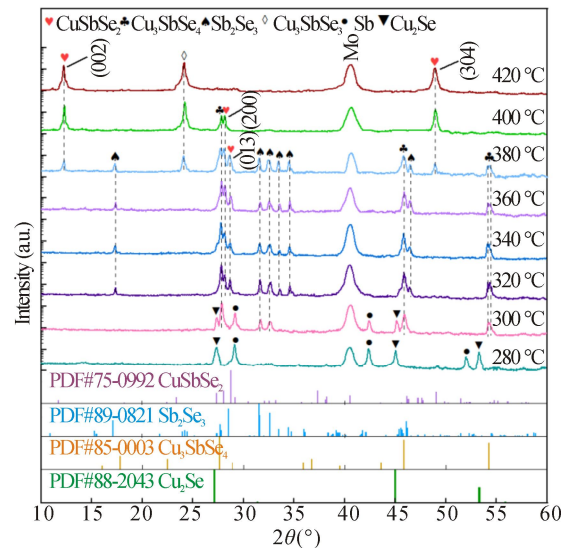
Fig.2 XRD patterns of thin films prepared with different annealing temperatures (280—420 °C)

The vibrational peak of CASe was present at 206 cm^{-1} with the temperature changed from 320 °C to 420 °C[32]. The intensity of CASe gradually increased with the increase of annealing temperature, and the strongest intensity of CASe was found at 360 °C. This indicated that CASe started to be generated at 320 °C and the crystallinity was best at 360 °C. The vibrational peak of Cu_3SbSe_4 was located at 187 cm[-1][33,34] and started to increase gradually with the increase of the annealing temperature. However, when the annealing temperature exceeds 360 °C, the intensity of Cu_3SbSe_4 started to weaken, and disappeared completely at 420 °C. The temperature rises to the CASe reaction temperature, resulting in the reduction of Cu_3SbSe_4. Besides, the vibrational peak of Sb_2Se_3 located at 251 cm^{-1} appeared simultaneously at 300 °C. A fainter vibrational peak of Sb_2Se_3 appeared at 372 cm^{-1} because of part of CASe decomposed when the annealing temperature increased to 380 °C[35]. However, The Sb_2Se_3 peak complete disappearance above 400 °C, which was attributed to its large saturation vapor pressure. Cu_3SbSe_3 originated from the decomposition of CASe, and its vibrational peak at 174 cm^{-1} appeared at 380 °C, after which the intensity of the vibrational peak increased rapidly with the increase of the annealing temperature. The peaks detected in Raman spectra were consistent with the XRD pattern.

Fig.4 shows SEM images of CASe films prepared at different annealing temperatures of 280 °C, 360 °C, 380 °C, and 420 °C, respectively. When the annealing temperature was 280 °C, Cu and selenium vapor reacted to form Cu_2Se, and Sb did not participate in the reaction. It can be observed in Fig.4(a) that the surface of the film

is rough. The generated hexagonal Cu_2Se grains embedded in the film, with a diameter of about 3 μm. There was unreacted Sb under Cu_2Se as shown in Fig.4(e), owing to the metal precursor was to electrodeposit Sb layer on Mo surface first, and Cu layer on Sb layer, Sb was unreacted with Se at 280 °C.
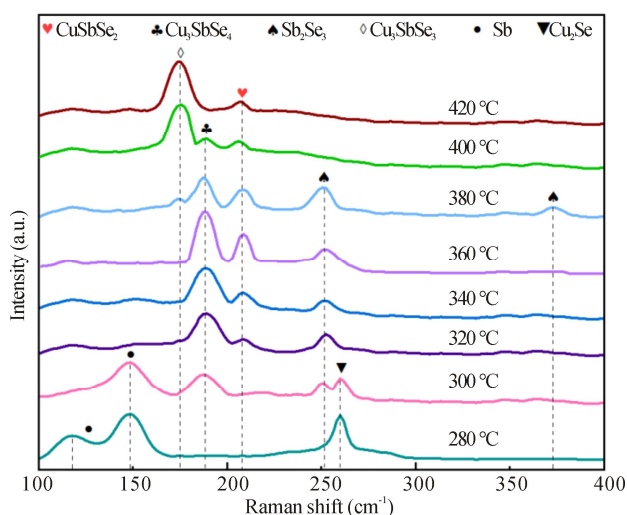
Fig.3 Raman scattering spectra of thin films prepared with different annealing temperatures (280—420 °C)

When the annealing temperature further increased to 360 °C, the film surface became compact and the film crystallization increased. It was worth noting that the obvious double-layer structure of the film was seen from the cross-sectional view of SEM (in Fig.4(f)). Combined with XRD and Raman scattering spectra, the top layer of the film was Cu_3SbSe_4 and the bottom layer was Sb_2Se_3. As the annealing temperature increased to 380 °C, the surface quality of the film became worse, cracks and pores appeared (Fig.4(c) and (g)). This may be due to the high vapor pressure of Se at 380 °C. Moreover, the separation phenomenon of the film was improved, and small amounts of rod-like grains began to appear, indicating CASe decomposed into Cu_3SbSe_3. When the annealing temperature increased to 420 °C, a very large rod-like structure formed on the surface of the film. Mo substrate was exposed (Fig.4(d)), owing to CASe decomposed. Additionally, the sublimation of Sb_2Se_3 led to volume shrinkage and pore formation during annealing treatment, which made the quality of the film worse.
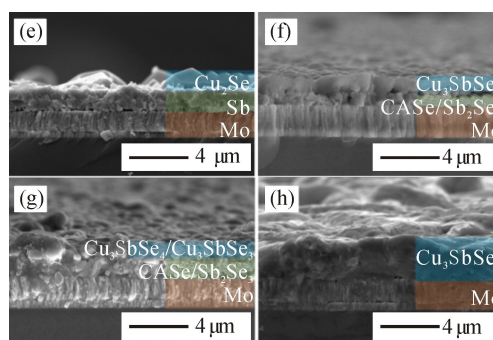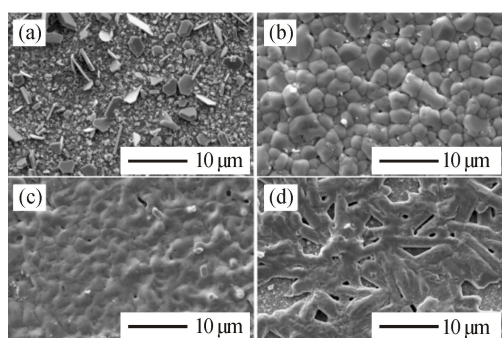
Fig.4 SEM surface and cross sections of CASe films prepared at different annealing temperatures: (a) (e) 280 °C; (b) (f) 360 °C; (c) (g) 380 °C; (d) (h) 420 °C

In order to study the effect of annealing temperature on the element composition of thin films, EDS of the samples were analyzed shown in Fig.4(e) and (f). Due to the obvious separation of thin films, the compositions located at blue and green boxes and all cross sections are recorded as e-1, e-2, e, f-1, f-2 and f, respectively. The sample compositions of Fig.4(g) and (h) were recorded as g and h. The tested compositions of each sample were listed in Tab.1.

Tab.1 Compositions of CASe films annealed at different temperatures

Sam-ple	Element ratio (at.%)			Compositional ratio (%)	
	Cu	Sb	Se	Cu/Sb	Se/(Cu+Sb)
e-1	56.87	14.78	28.35	3.85	0.40
e-2	7.37	76.49	16.14	0.10	0.19
e	31.24	46.09	22.67	0.68	0.29
f-1	37.42	12.96	49.62	2.89	0.98
f-2	12.26	39.23	48.51	0.31	0.94
f	24.93	26.05	49.02	0.96	0.96
g	27.35	23.82	48.83	1.15	0.95
h	34.06	19.23	46.71	1.77	0.88

As listed in Tab.1, when the annealing temperature was 280 °C (sample e), the atomic percent of Se at the bottom of the film was only 16.14%, due to the insufficient selenization reaction at low annealing temperature. The atomic percent of Cu/Se on the surface of the film was close to 2: 1, and the atomic percent of Sb at the bottom was about 76.49%, indicating the formation of Cu_2Se and unreacted Sb were existed. With the annealing temperature increased to 360 °C (samples f-1 and f-2), the atomic percent of Cu, Sb, and Se on the surface and bottom was close to the chemical ratio of Cu_3SbSe_4 and Sb_2Se_3. The overall ratio of sample f was close to the chemical ratio of CASe. With the further increase of annealing temperature, the ratio of Cu/Sb gradually increased to 1.77, indicated that Sb lost due to the sublimation of Sb_2Se_3 at high temperature. The above results are consistent with the results of XRD and Raman analysis.

360 °C was chosen as the annealing temperature to prepare CASe.

The conclusions of phase evolution in this section were summarized in Tab.2. From what has been discussed above, CASe compounds will be formed only when the annealing temperature is higher than 320 °C. The crystallinity of CASe is the highest with the annealing temperature between 360 °C and 380 °C. The temperature stability range of CASe in this work was about between 360 °C and 380 °C. In Se-rich environment, a competitive relationship between Cu_3SbSe_4 generation and CASe was existed. Cu_3SbSe_4 began to form at 300 °C. CASe would be decomposed into Cu_3SbSe_3 and Sb_2Se_3 at high temperature (400 °C or above), Sb_2Se_3 volatilized from the film, resulting in poor surface quality of cracks and holes. The phase and crystal orientation were changed when the annealing temperature changed.

Tab.2 Phase evolution of thin films at different annealing temperatures

Annealing temperature (°C)	Phase composition	Preferred orientation of CASe
280	Cu_2Se+Sb	
300	$Cu_3SbSe_4+Sb_2Se_3+$ Cu_2Se+Sb	—
320	$CuSbSe_2+Cu_3SbSe_4+$ Sb_2Se_3	(200)
340		
360		
380	$CuSbSe_2+Cu_3SbSe_3+$	(200)
400	$Cu_3SbSe_4+Sb_2Se_3$	(002)(304)
420	$CuSbSe_2+Cu_3SbSe_3$	(002)(304)

In the previous section, there was obvious layer separation in the CASe films. The top layer was Cu_3SbSe_4, the bottom layer was Sb_2Se_3, and no pure CASe phase film was formed. The stratification phenomenon was similar to the experimental results of Ref.[19]. PENEZKO et al[19] showed a double-layer structure film. The results believed that the decomposition of CASe into Cu_3SbSe_4 and Sb_2Se_3 led to the formation of double-layer structure. The grains at the top of the film grew gradually with the increase of annealing temperature and annealing time. On the above analysis, 360 °C was selected as the annealing temperature to study the effect of selenization time on the compositions of the films.

XRD was carried out on CASe thin films prepared with different selenization time. Fig.5 shows the XRD patterns of thin films with selenization time of 2 min, 5 min, 10 min, 20 min, 30 min, 40 min, and 50 min. When the selenization time was 2 min, the phases of the film were consisted of Cu_2Se, Sb and Sb_2Se_3. Owing to Se permeated downward from the film surface, Se reacted preferentially with the top Cu layer of the metal precursor to form Cu_2Se, and then reacted with Sb under the Cu layer to form Sb_2Se_3. Since the selenization time

was short, Se vapor reacted with Sb incompletely. The intensity of Sb and Cu_2Se diffraction peaks weakened with the selenization time prolonged to 5 min, indicating more Sb and Cu_2Se were involved in the reaction. The main peak of Cu_3SbSe_4 at 27.43° and the peaks at 45.44° and 53.87° began to appear, the peaks at 31.66° and 32.64° were corresponded to Sb_2Se_3. The diffraction peak of CASe at 28.08° was weak. Sb_2Se_3 formed by the reaction of Sb with Se vapor. Cu_2Se reacted with Sb_2Se_3 to form Cu_3SbSe_4 in an Se-rich atmosphere. When the selenization time was 10 min, the CASe peak increased obviously, and the peak of Sb and Cu_2Se disappeared, Sb reacted with Se to form Sb_2Se_3, and Sb_2Se_3 reacted with Cu_2Se to form Cu_3SbSe_4 and CASe. The intensity of CASe peak was the strongest, indicating the crystallinity was high, when the selenization time was prolonged to 20 min. At the same time, the Sb_2Se_3 peak at 16.98°, 33.89° and 34.31° began to appear. When the selenization time was 30 min to 50 min, the CASe peak intensity decreased with the increase of selenization time, indicating too long selenization time reduced the crystallinity of CASe. In this experiment, the optimal selenization time was set at 20 min.
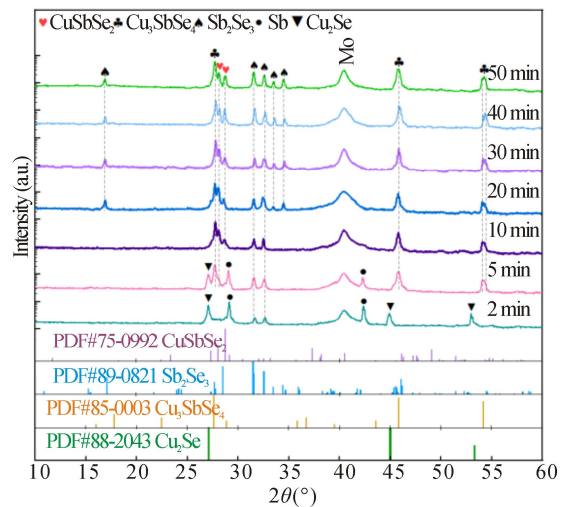
Fig.5 XRD patterns of thin films prepared with different selenization time (2—50 min)

The samples prepared with different selenization time were further analyzed by Raman scattering spectra, as shown in Fig.6. The vibration peak, sample with selenization time of 2 min, at 116 cm^{-1} and 150 cm^{-1} corresponds to the vibration peak of Sb. The peak at 260 cm^{-1} corresponds to Cu_2Se. The tiny vibration peak at 250 cm^{-1} corresponds to Sb_2Se_3. It is proved that the selenization reaction began from the surface of the film and gradually went to the bottom of the film. When the selenization time was 5 min, the vibration peak at 188 cm^{-1} corresponding to Cu_3SbSe_4 began to appear, the Sb and Cu_2Se peak became weak, and the Sb_2Se_3 peak became strong. However, the characteristic vibration peak at 208 cm^{-1} corresponding to CASe was not found, due to

the poor crystallinity of CASe and its deep position in the film. With the extension of selenization time, Sb and Cu_2Se disappeared, Cu_3SbSe_4 and Sb_2Se_3 did not change. The CASe peak reached the strongest when the selenization time was 20 min, and the crystallinity of CASe was the highest, which was the same as that of XRD.
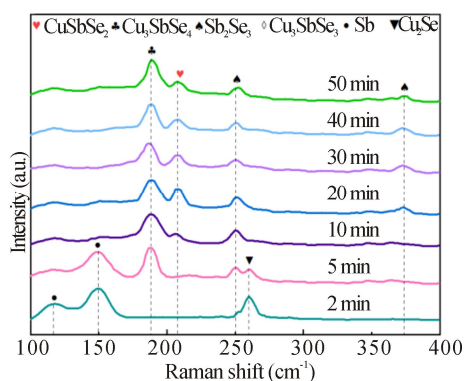
Fig.6 Raman scattering spectra of thin films prepared with different selenization time (2—50 min)

Fig.7 shows the SEM cross sections of CASe thin films prepared with different selenization time (2 min, 10 min, 20 min, 30 min and 50 min, respectively). In Fig.7, the separation phenomenon of the films was more obvious with the selenization time increase. The reactions selenized 2 min and 10 min were not sufficient. The bottom grains of the films selenized 30 min and 50 min were fine with a lot of pores. This is because too long selenization time led to the decomposition of antimony selenide and the loss of selenium. The separation of the thin films may be caused by the preferential formation of Cu_3SbSe_4.
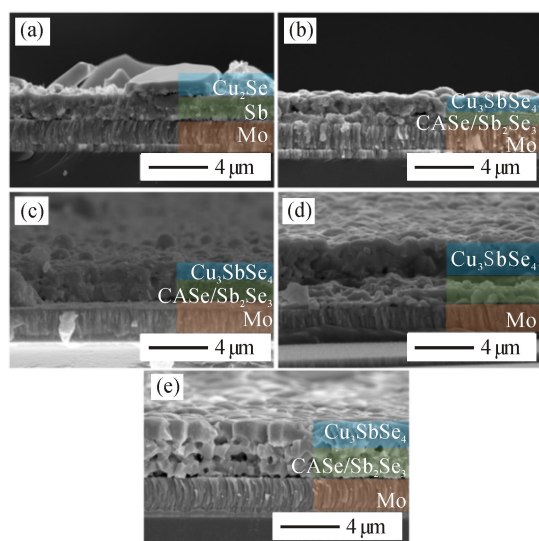
Fig.7 SEM cross sections of CASe thin films prepared with different selenization time: (a) 2 min; (b) 10 min; (c) 20 min; (d) 30 min; (e) 50 min

Additionally, the adhesion between the top layer and

the bottom layer of CASe was worse than that between the bottom layer and the Mo substrate. The tape experiment based on 20 min selenide thin film was carried out. The surface of the film was characterized by SEM and EDS line scanning as shown in Fig.8. The yellow line shows the edge of the tape, that is, the area on the left side of the yellow line has been treated with tape, and the EDS line scanning was in the direction of the red line arrow. It can be found that the Cu content of the film on the left side of the yellow line is low. On the right side of the yellow line, Cu and Se contents increases, while the Sb content decreases, indicating the film has a double-layer structure. The top layer is copper-rich, and the bottom layer is copper-poor, selenization reaction first occurred on the top surface of the film.
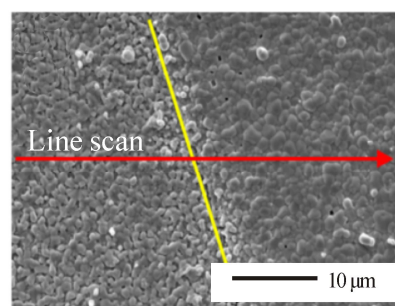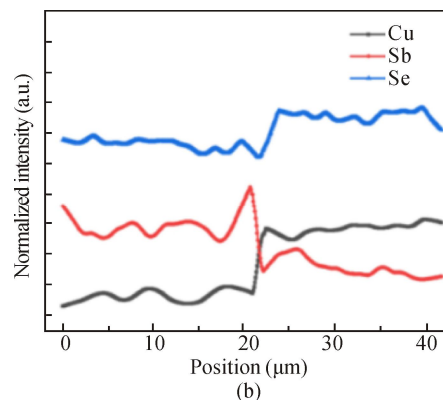
Fig.8 (a) SEM and (b) EDS line scan characteristic diagrams of CASe thin film for tape experiment

From the above analysis, it can be seen that obvious layer separation was formed during the selenization process of CASe thin films, with the top layer of Cu_3SbSe_4 and the bottom layer of Sb_2Se_3. This not only affects the formation of CASe, but leads to the increase of grain boundaries and recombination centers.

In order to study the film separation, the state of metal precursor was investigated. The precursor after electrodeposition was heated to 200 °C with 20 min in a tube furnace and kept for 5 min. XRD analysis was carried out, as shown in Fig.9. In the as-deposited metal precursor, there were three kinds of phases Cu_2Sb, Cu, and Sb. Among them, the diffraction peak of Cu (JCPDS: 89-2838) was the strongest, with corresponding peak

position at 43.41° and 50.49°. There was a weak diffraction peak of Sb at 23.81° and a diffraction peak of Cu_2Sb (JCPDS: 87-1176) at 26.89°, 31.81°, 35.14°, and 45.35°. The formation of Cu_2Sb alloy may be due to the high deposition energy during the electrodeposition process. After the metal precursor was annealed at 200 °C, the diffraction peak of Cu disappeared, the main peak of Sb was sharp at 28.82°, and the half peak width decreased. The peaks at 42.06° and 51.66° corresponded to the diffraction peak of Sb. The intensity of Cu_2Sb peak was enhanced, indicating the alloy degree between Cu and Se was increased.

Se permeates downward from the film surface, Cu_3SbSe_4 begins to form when the annealing temperature is 300 °C, lower than the formation temperature of CASe. The initial heating rate was only 10 °C/min. It took a long time to stay in the temperature range of Cu_3SbSe_4 formation, which led to the separation of the films. To improve the separation of CASe films, annealing rates were changed to 20 °C/min and 30 °C/min to limit the formation of Cu_3SbSe_4.
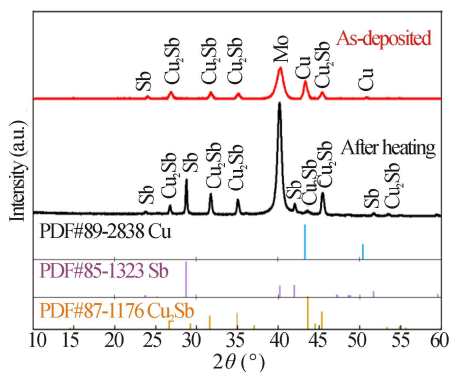
Fig.9 Comparison of XRD patterns of metal preform after electrodeposition and heating

Fig.10 shows the XRD patterns of the films prepared with different annealing rates. With the increase of the heating rate, the intensity of the CASe diffraction peak at 27.95° increased gradually, and the intensity of Cu_3SbSe_4 at 27.40° decreased obviously. The intensity of the secondary peak at 45.41° becomes very weak, and the diffraction peak at 53.79° disappears at the heating rate of 30 °C/min. This is because the duration time to reach the CASe formation temperature is shortened, the reaction time for the formation of Cu_2Sb and Cu_3SbSe_4 is reduced, which is beneficial to form CASe and effectively improve the layer separation of CASe films.

Fig.11 shows the SEM images of CASe films prepared with different heating rates of 10 °C/min, 20 °C/min and 30 °C/min, respectively. The layer separation of the CASe prepared with 10 °C/min was obvious. Dense and large-grained layer was formed on the film surface, and fine grains were formed at the bottom. The separation phenomenon of the film prepared with 20 °C/min was improved obviously, and the grains were more compact.

With the increase of heating rate of 30 °C/min, the separation phenomenon of the film was further improved and the pores at the bottom contact were reduced, owing to the uniform distribution of elements. Increasing the heating rate reduced the aggregation of Cu on the surface and obviously improved the phase separation of the thin films. The sample quality with a heating rate of 30 °C/min was the best, and the grains were more compact and uniform.
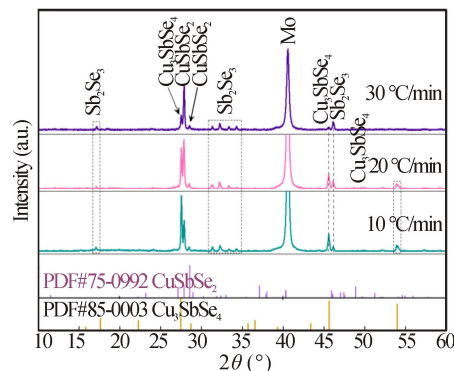
Fig.10 XRD spectra of thin films prepared with different heating rates (10—30 °C/min)
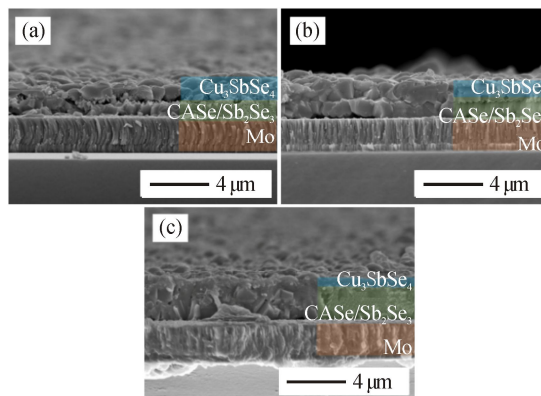
Fig.11 SEM cross sections of CASe thin films prepared with different heating rates: (a) 10 °C/min; (b) 20 °C/min; (c) 30 °C/min

In this work, selenization annealing of Sb/Cu metal layer to prepare CASe thin films with pulse electrodeposition process was studied, and the growth mechanism of CASe film was analyzed. Cu and Sb reacted with Se to form Cu_2Se and Sb_2Se_3, respectively. Then Cu_2Se and Sb_2Se_3 reacted further to generate CASe. The preferred orientation was CASe (200) crystal plane. When the annealing temperature was too high, CASe decomposed to form Cu_3SbSe_3 and Sb_2Se_3. Since the temperature of producing Cu_3SbSe_4 (300 °C) was lower than that of CASe (320 °C), the preferential formation of Cu_3SbSe_4 leads to layer separation. By increasing the heating rate to 30 °C/min, the separation of CASe thin films was improved. Finally, the CASe thin films with relatively high crystallinity were obtained at 360 °C with heating rate of

30 °C/min and selenization time of 20 min.

Ethics declarations

Conflicts of interest

The authors declare no conflict of interest.

References

[1]   NAKAMURA M, YAMAGUCHI K, KIMOTO Y, et al. Cd-free Cu(In,Ga)(Se,S)$_2$ thin-film solar cell with record efficiency of 23.35%[J]. IEEE journal of photovoltaics, 2019, 9(6)：1863-1867. GREEN M, DUNLOP E, HOHL-EBINGER J, et al. Solar cell efficiency tables (version 57)[J]. Progress in photovoltaics, 2021, 29(1)：3-15.

[2]   GREEN M, DUNLOP E, HOHL-EBINGER J, et al. Solar cell efficiency tables (version 57)[J]. Progress in photovoltaics, 2021, 29(1)：3-15.

[3]   LIN L, CHEN G, YAO L, et al. Antimony loss and composition-dependent phase evolution of CuSbS$_2$ absorber using oxides nanoparticles ink[J]. Materials science in semiconductor processing, 2021, 133：105944.

[4]   GEIM A. Graphene：status and prospects[J]. Science, 2009, 324：1530-1534.

[5]   PHAM P, BODEPUDI S, SHEHZAD K, et al. 2D heterostructures for ubiquitous electronics and optoelectronics：principles, opportunities, and challenges[J]. Chemical reviews, 2022, 122：6514-6613.

[6]   HADKE S, HUANG M, CHEN C, et al. Emerging chalcogenide thin films for solar energy harvesting devices[J]. Chemical reviews, 2021, 122：10170-10265.

[7]   MAJSZTRIK P, KIRKHAM M, GARCIA-NEGRON V, et al. Effect of thermal processing on the microstructure and composition of Cu-Sb-Se compounds[J]. Journal of materials science, 2013, 48：2188-2198.

[8]   ZHANG Y, OZOLINS V, MORELLI D, et al. Prediction of new stable compounds and promising thermoelectrics in the Cu-Sb-Se system[J]. Chemistry of materials, 2014, 26：3427-3435.

[9]   LIN W, WANG N, LAN Z, et al. A facile ion-exchange assisted chemical bath deposition of CuSbS$_2$ for thin film solar cells[J]. Solar energy, 2022, 244：465-473.

[10]   ABOUABASSI K, SALA A, ATOURKI L, et al. Electrodeposited CuSbSe$_2$ thin films based solar cells on various substrates[J]. Journal of nanoparticle research, 2022, 24：1-10.

[11]   TANG D, YANG J, LIU F, et al. One-step electrodeposition and annealing of CuSbSe$_2$ thin films[J]. Electrochemical and solid state letters, 2012, 15：D11-D13.

[12]   RAHMAN A, BHATTACHARYA A, SARMA A. Synthesis of Cu$_3$SbS$_4$, Cu$_3$SbSe$_4$ and CuSbTe$_2$ thin films via chalcogenation of sputtered Cu-Sb metal precursors[J]. Thin solid films, 2022, 754：139315.

[13]   WELCH A, BARANOWSKI L, ZAWADZKI P, et al. CuSbSe$_2$ photovoltaic devices with 3% efficiency[J].

Applied physics express, 2015, 8：082301.

[14]   WELCH A, BARANOWSKI L, PENG H, et al. Trade-offs in thin film solar cells with layered chalcostibite photovoltaic absorbers[J]. Advanced energy materials, 2017, 7：1601935.

[15]   YANG B, WANG C, YUAN Z, et al. Hydrazine solution processed CuSbSe$_2$：temperature dependent phase and crystal orientation evolution[J]. Solar energy materials and solar cells, 2017, 168：112-118.

[16]   WANG C, YANG B, DING R, et al. Reactive close-spaced sublimation processed CuSbSe$_2$ thin films and their photovoltaic application[J]. APL materials, 2018, 6：084801.

[17]   RAMPINO S, PATTINI F, BRONZONI M, et al. CuSbSe$_2$ thin film solar cells with ~4% conversion efficiency grown by low-temperature pulsed electron deposition[J]. Solar energy materials and solar cells, 2018, 185：86-96.

[18]   YAN H, XIAO R, PEI Y, et al. Structural, electrical and optical characteristics of CuSbSe$_2$ films prepared by pulsed laser deposition and magnetron sputtering processes[J]. Journal of materials science-materials in electronics, 2020, 31：644-651.

[19]   PENEZKO A, KAUK-KUUSIK M, VOLOBUJEVA O, et al. Properties of Cu-Sb-Se thin films deposited by magnetron co-sputtering for solar cell applications[J]. Thin solid films, 2021, 740：139004.

[20]   GOYAL D, GOYAL C, IKEDA H, et al. Study of CuSbSe$_2$ thin films grown by pulsed laser deposition from bulk source material[J]. Materials science in semiconductor processing, 2021, 121：105420.

[21]   ABOUABASSI K, ATOURKI L, SALA A, et al. Annealing effect on one step electrodeposited CuSbSe$_2$ thin films[J]. Coatings, 2022, 12：75.

[22]   KIM S, KIM N. Impurity phases and optoelectronic properties of CuSbSe$_2$ thin films prepared by co-sputtering process for absorber layer in solar cells[J]. Coatings, 2020, 10：14.

[23]   GOYAL D, GOYAL C, IKEDA H, et al. Role of growth temperature in photovoltaic absorber CuSbSe$_2$ deposition through e-beam evaporation[J]. Materials science in semiconductor processing, 2020, 108：104874.

[24]   GUO T, WANG D, YANG Y, et al. Preparation and characterization of CuSbSe$_2$ thin films deposited by pulsed laser deposition[J]. Materials science in semiconductor processing, 2021, 127：105716.

[25]   REINHARD P, BUECHELER S, TIWARI A. Technological status of Cu(In,Ga)(Se,S)$_2$-based photovoltaics[J]. Solar energy materials and solar cells, 2013, 119：287-290.

[26]   HUANG Y, ZHANG B, LI J, et al. Unconventional doping effect leads to ultrahigh average thermoelectric power factor in Cu$_3$SbSe$_4$-based composites[J]. Advanced materials, 2022, 34：2109952.

[27] SCOTT W, KENCH J. Phase diagram and properties of Cu_3SbSe_4 and other $A_3^IB^VC_4^{VI}$ compounds[J]. Materials research bulletin, 1973, 8：1257-1267.

[28] TANG R, CHEN S, ZHENG Z, et al. Heterojunction annealing enabling record open-circuit voltage in antimony triselenidesolar cells[J]. Advanced materials, 2022, 34：2109078.

[29] WITTE W, KNIESE R, POWALLA M. Raman investigations of Cu(In, Ga)Se$_2$ thin films with various copper contents[J]. Thin solid films, 2008, 517：867-869.

[30] ISHIZUKA S. Impact of Cu-deficient pn heterointerface in CuGaSe$_2$ photovoltaic devices[J]. Applied physics letters, 2021, 118：133901.

[31] XUE D, YANG B, YUAN Z, et al. CuSbSe$_2$ as a potential photovoltaic absorber material：studies from theory to experiment[J]. Advanced energy materials, 2015, 5：9.

[32] WANG W, WANG Y, BO L, et al. Enhanced thermoelectric properties of Cu_3SbSe_4 via compositing with nano-SnTe[J]. Journal of alloys and compounds, 2021, 878：160358.

[33] WANG C, WU Y, PEI Y, et al. Dynamic disorder phonon scattering mediated by Cu atomic hopping and diffusion in Cu_3SbSe_3[J]. Npj computational materials, 2020, 6：155.

[34] EFTHIMIOPOULOS I, ZHANG J, KUCWAY M, et al. Sb$_2$Se$_3$ under pressure[J]. Scientific reports, 2013, 3：2665.

[35] TIWARI K, VINOD V, SUBRAHMANYAM A, et al. Growth and characterization of chalcostibite CuSbSe$_2$ thin films for photovoltaic application[J]. Applied surface science, 2017, 418：216-224.